Analysis and Experiments of a Haptic Telemanipulation Environment for a Microrobot Driven by Centripetal Forces

Kostas Vlachos
e-mail: kostaswl@central.ntua.gr

Evangelos Papadopoulos
e-mail: egpapado@central.ntua.gr

Department of Mechanical Engineering,
National Technical University of Athens,
Heroon Polytechniou 9,
15780 Athens, Greece

This paper presents the analytical and experimental results on a new haptic telemanipulation environment for microrobot control. The proposed environment is comprised of a 5DOF force feedback mechanism, acting as the master, and a 2DOF microrobot, acting as the slave. The fact that the slave microrobot is driven by two centripetal force vibration micromotors makes the presented telemanipulation environment exceptional and challenging. The unique characteristics and challenges that arise during the haptic micromanipulation of the specific device are described and analyzed. The developed solutions are presented and discussed. Several experiments show that, regardless of the disparity between the master and slave, the proposed environment facilitates functional and simple microrobot control during micromanipulation operations.
[DOI: 10.1115/1.2988385]

1 Introduction

Recently, research in the area of robotic manipulation in the micro- and nanoworlds has gained a lot of interest and importance. The research activity focuses on areas, such as microsurgery, direct medical procedures on cells, biomechatronics, micromanufacturing, and micro-assembly, where tele-operated microrobotic devices can be used. It is well known now that not only the visual but also the haptic feedback can be helpful for a successful tele-operated micromanipulation procedure [1]. Therefore, some of the master manipulators are haptic devices, able to drive the microrobots and at the same time to transmit torques and forces to the operator.

A haptic tele-operation system, for use in microsurgery, was presented by Salcudean and Yan [2] and by Salcudean et al. [3]. Their system consists of two magnetically levitated and kinematically identical wrists, acting as a macromaster and a microslave, and a conventional manipulator that transports them. A telenanorobotics system using an atomic force microscope (AFM), as the nanorobot, has been proposed by Sitti and Hashimoto [4]. The system provides a 1DOF force feedback device for haptic sensing, using a linear scaling approach. A microsurgical telerobot is presented, which consists of a 6DOF parallel micromanipulator attached to a macromotion industrial robot and a 6DOF haptic master device [5]. The system provides a disturbance observer to enhance the operator's perception.

A microtele-operation system for tasks, such as micro-assembly or micromanufacturing, was developed by Ando et al. [6]. The haptic master is a 6DOF serial link mechanism, and the slave is a parallel link mechanism. Alternatively the Phantom, a commercial haptic interface, can be used as a master device [7]. The Phantom was used as a haptic master by Menciassi et al. [8] where a microinstrument for microsurgery or minimally invasive surgery was tested. Sitti et al. [9] used the same haptic interface to tele-operate a piezoresistive atomic force microscope probe used as a slave manipulator and force sensor. A biomicromanipulation system for biological objects, such as embryos, cells, or oocytes, was presented in Ref. [10]. The system uses the Phantom to provide an augmented virtual haptic feedback during cell injection. A similar system for microinjection of embryonic stem cells into blastocysts is described in Ref. [11], although the system has no haptic feedback. The mechanical design of a haptic device integrated into a mobile nanohandling station is presented in Ref. [12]. The Delta haptic device was proposed as a nanomanipulator in Ref. [13]. The device is also interfaced to an AFM.

The scaling problem in macro-micro bilateral manipulation has been discussed by Colgate [14], where a condition for the robust stability of an operator/bilateral manipulator/environment system is derived using the structured singular value. Goldfarb [15] addressed the issue of dynamic similarity and intensive property invariance in scaled bilateral manipulation. Using dimensional analysis methods yields a force-scaling factor that minimizes the intensive distortion of the environment. A force feedback control system for micro-assembly focusing on the issues of force transmission and control was presented [16]. Park and Khatib [17] presented a tele-operation approach using a virtual spring and a local contact force control on the slave robot. Faulring et al. [18] developed an algorithm that enables the haptic display of constrained dynamic systems via admittance displays.

For a successful coordination between the master and slave, an appropriate telemanipulation environment is required, especially when the two have a disparate structure. This may happen in cases in which we need to manipulate different slave devices with the same master haptic mechanism, as for example in microsurgery, in micro-assembly, or in micromanipulation. Obviously, this has economic benefits too. In this paper the master and slave mechanisms are not only structurally disparate, but in addition, they function at a different scale. These characteristics make the telemanipulation, as described above, a particularly challenging issue.

In the proposed haptic environment, the commanding master device is a 5DOF force feedback mechanism, while the executing slave is a 2DOF microrobot with special behavior and is driven by two centripetal force actuators. Although the haptic master employed is a haptic mechanism designed for the human hand, and therefore shares characteristics with other such devices, to the knowledge of the authors, it is the first time that a vibration driven micro-robotic device is considered as the slave. This slave mechanism has a number of advantages relative to other microrobotic devices; namely, it is characterized by a low cost, complexity, and

Contributed by the Engineering Simulation and Visualization Committee of ASME for publication in the Journal of Computing and Information Science in Engineering. Manuscript received September 30, 2007; final manuscript received June 30, 2008; published online xxxxx-xxxxx-xxxxx. Guest Editor: J. Oliver, M. Omalley, and K. Kesavadas.

Copyright © 2008 by ASME

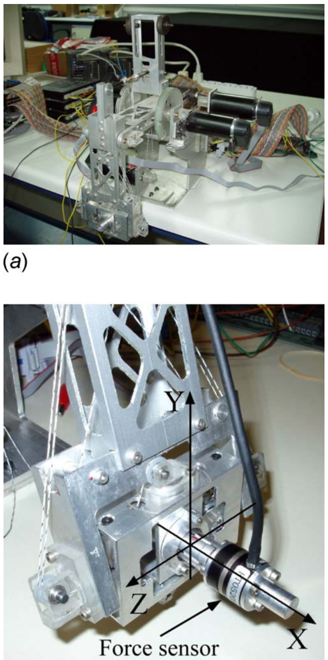

Fig. 1 The haptic master (*a*) and its force sensor-equipped spherical joint (*b*)

power consumption. The special characteristics and challenges that arise due to the unique design of the microrobotic device during haptic micromanipulation are described and analyzed. This design has implications not only the device's motion, but also on the forces that appear during micromanipulation. Note here that the particular design of the microrobot rules out any consideration of designing a special haptic master dedicated to the particular slave microrobot. The developed solutions are presented and discussed. Two communication channels are identified and their integrated input modes and force phases are described in detail. The use of the proposed haptic telemanipulation environment is illustrated by several experiments. These show that, regardless of the disparity between master and slave, the proposed environment facilitates functional and simple to the user microrobot control during micromanipulation operations.

The proposed environment represents a first step in developing a unified framework for the manipulation of devices with disparate structure and scale using haptic technologies. These devices can be robotic mechanisms of any degrees of freedom (DOF), holonomic or nonholonomic vehicles, or linear or nonlinear systems. They can follow a path or interact with their environment and must be commanded through a haptic interface. The reason for this can be the size of the manipulation device (too big for human capabilities), the distance between the human and the device (control of an exploration rover), the scale of the manipulation environment (a microrobotic device for tissue inspection), the potential risk for the human or the device, (a mobile platform in a nuclear facility), or the physical nature of the manipulated device (for example, a simulated virtual environment).

2 Master and Slave Brief Description

The developed haptic telemanipulation environment employs an existing 5DOF haptic mechanism as the master and a 2DOF microrobotic platform driven by two centripetal force actuators as the slave. A brief description of the master and slave is given next.

2.1 Master Haptic Device. The master device is the haptic mechanism shown in Fig. 1. It consists of a 2DOF five-bar linkage and a 3DOF spherical joint. All DOF are active. To reduce the mechanism moving the mass and inertia, all actuators are placed at the base. The transmission system is implemented using tendon drives with capstans. The device is thoroughly described, including kinematics and dynamics, in Ref. [19]. Although this haptic device was not developed for micromanipulation, it is suitable since it was designed optimally to exhibit maximum transparency, as seen from the operator side [20]. Fig. 1(*b*) shows the macroworld coordination system, i.e., the master haptic device system. The mechanism can translate in the X and Y axes by 10 cm and rotate about the X axis by ± 180 deg and about the Y and Z axes by ± 30 deg maintaining at the same time its good functionality.

2.2 Slave Microrobotic Platform. The slave device, shown in Fig. 2(*a*), is a microrobotic platform employing two vibration micro-actuators. This novel motion mechanism exploits the centripetal forces generated by eccentric masses that are rotated by motors mounted on a platform. The angular speed of these motors is controlled, so that the generated centripetal forces induce to the platform a desirable motion. The interaction of centripetal forces with frictional forces developed at contact points yields a stepwise motion of the platform. The magnitude of the net displacement per step is controlled by the rotational speed of the eccentric load and can be made arbitrarily small. This way micromotion can easily be achieved. The concept was inspired by observing the motion of devices that vibrate, such as cellular phones or unbalanced washing machines. The platform is described in detail, including the design, kinematics, dynamics, and control, in Ref. [21]. It is a novel totally enclosed design with applications in the areas of micro-assembly, biomechatronics, microsurgery, etc.

The platform can perform translational and rotational sliding with submicrometer positioning accuracy and velocities of up to 1.5 mm/s. All the components of the mechanism, including its

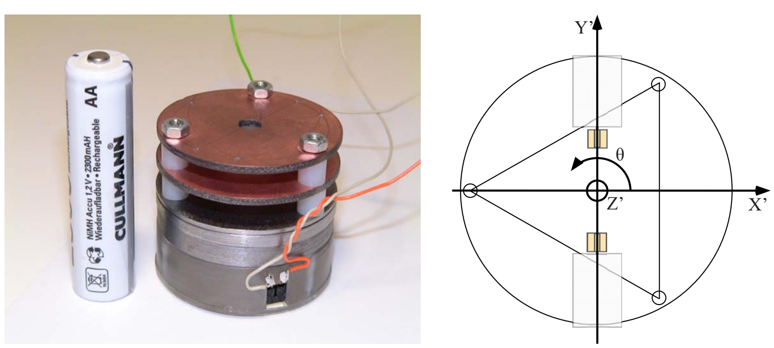

Fig. 2 The slave microrobotic platform (*a*) and the microworld coordination system (*b*)

driving units, are of low cost and are readily available. The total cost of the platform does not exceed 50 euros. In Fig. 2(*b*), the microworld coordination system is shown. The platform translates along the X' axis and rotates about the Z' axis by an angle θ.

3 Haptic Telemanipulation System Features and Requirements

3.1 Slave Microrobot Features. The design and special features of the slave microrobotic platform (microrobot) introduce a number of challenges that need to be tackled by the telemanipulation environment design. These are presented next.

AQ: #1

1. The microrobot is enabled for coarse and fine motions. It is a mobile platform designed to perform fine tasks, such as assembling parts at the microscale in cooperation with other similar microrobots. Furthermore, to avoid the need to be transported by an additional macrorobotic mechanism, it is designed with the capability for coarse high-speed motions during large displacements toward a target. Its translational sliding velocity is up to 1.5 mm/s.
2. The slave microplatform and the master haptic device are kinematical dissimilar. The former is a 2DOF mobile platform and the latter is a 5DOF robotic mechanism.
3. The inverse kinematics of the nonlinear microrobot is not available in real time. In addition, the microrobot exhibits complex nonholonomic characteristics.
4. The vibration actuators must operate within a specific speed range (rpm). The theoretical upper limit depends on the type of the ground and results in the maximum translational velocity. When this limit is exceeded, the microrobot exhibits an additional undesirable vertical vibration. The practical upper limit is taken to be about 80–90% of the theoretical limit. A low rpm limit also exists and is due to the need to overcome the support frictional forces, so that net motion may result.
5. To achieve sub micrometer positioning accuracy, the microrobot has the option to drive alternatively the two vibration micro-actuators.
6. The forces applied on the microtargets can be smooth or, due to the vibrating nature of the actuation, can be in the form of impacts.

AQ: #2

3.2 Master Haptic Device Requirements. The above slave microrobot features dictate the following requirements for the master haptic device.

1. The master haptic device has to drive the microplatform (*a*) toward the target in coarse motion and (*b*) during micromanipulation in fine motion. During the coarse motion phase, a high speed and low positioning accuracy is needed, while the opposite is true during fine motion.
2. To resolve the kinematical dissimilarity between the master and the slave, taking into account that an inverse kinematics relationship is unavailable in real time, a mapping from the master haptic device Cartesian space to the microrobot actuator space has to be developed.
3. The master must send independent commands to each actuator. In addition, the ability to drive each micro-actuator alternatively is needed. In general, capabilities for (*a*) pure translation, (*b*) pure rotation, and (*c*) combined planar motion must be available.
4. A suitable micro/macro force mapping has to be defined. The force feedback mechanism should transfer the microenvironment forces to the macro-environment operator forces according to an appropriate function. This function must be able to handle not only smooth forces, but impact forces as well.

Next, the implementation of the above requirements to the haptic telemanipulation environment is described.

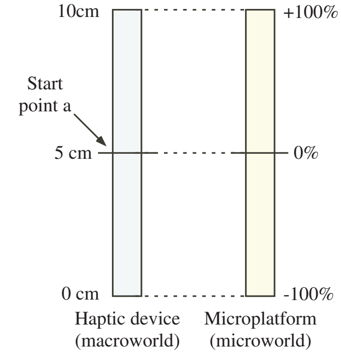

Fig. 3 The MaIM input scheme

4 Haptic Telemanipulation Environment Analysis

In the haptic telemanipulation environment, the master haptic device and the slave microplatform communicate bilaterally. The first communication channel transmits motion commands from the haptic mechanism to the microrobot. PWM circuits drive the microplatform actuators, according to the percentage (0–100%) of their duty cycle. As a result, actuator angular velocities are set and produce microrobot translations and rotations. Consequently the output of the master haptic device should be the percentage (0–100%) of the PWM duty cycle. The input to the haptic mechanism is the command given by the operator's hand. AQ: #3

The second communication channel transmits forces from the microrobot to the haptic mechanism. Its input is the microforces sensed by the microrobot during manipulation. The output of this channel is the force that the haptic device applies to the operator. Next, the communication channels are analyzed further.

4.1 First Communication Channel. In order to realize the first communication channel, the following three mutually exclusive input modes are defined. The first is the macroscopic input mode (MaIM), the second is the macroscopic rotation input mode (MRIM), and the third is the microscopic input mode (MiIM). The operator can choose and control the modes from the appropriate software. Our goal in the first two input modes is to achieve coarse motion of the platform, while in the third mode, it is to achieve fine micromanipulation.

4.1.1 The Macroscopic Input Mode. The master haptic manipulator uses this mode in order to drive the microrobotic platform toward the microtarget in linear or curved coarse motion. In this mode the positive/negative translation of the master haptic device end-effector in the X axis results in an increase in the positive/negative rotational speed of *both* microrobot vibration micro-actuators and therefore results in microrobot translation along the X axis.

To obtain a curved translation, a difference in the micro-actuator rotational velocities must exist. This is achieved by rotating the haptic device end-effector about the Y axis. A positive/negative rotation about this axis results in an increase in the rotational speed of the first/second micro-actuator.

As mentioned earlier, the haptic device end-effector can translate in the X axis by 10 cm and rotate about the Y axis by about ± 30 deg. Therefore, the start point of the end-effector is taken at the middle of its possible displacement, see Fig. 3, point a. A translation of the haptic device end-effector from start point a results in a percentage command of the micro-actuator speeds q according to

$$q = 20(p - 5) \quad (\%) \tag{1}$$

where p (cm) is the haptic device end-effector position.

Table 1 Haptic telemanipulation environment input modes

	MaIM		MRIM		MaIM	
In X positive	+	+	+	−	+	+
In X negative	−	−	−	+	−	−
About Y positive	↑	0	↑	0	1	0
About Y negative	0	↑	0	↑	0	1
	Microat. A	Microat. B	Microat. A	Microat. B	Microat. A	Microat. B

Additionally, for each degree (deg) of end-effector rotation about the Y axis, the corresponding micro-actuator speed is increased by 1%.

4.1.2 The Macroscopic Rotation Input Mode. The master haptic device uses this mode to rotate the microrobot without translation, again in coarse motion. This mode is useful in changing fast the direction of microplatform motion, and can be achieved by rotating the micro-actuators in equal and opposite speeds. To this end, the master operator translates the end-effector along the X axis resulting in an increase in the rotational speed of both micro-actuators, but this time with an opposite speed direction.

4.1.3 The Microscopic Input Mode. The master haptic device uses this mode during micromanipulation. This mode is useful after the microplatform has reached the microtarget and is starting micromanipulations. Two alternative ways were examined for this mode. The first is to function the haptic device in MaIM, such as in the macroscopic case, but with low actuator velocities. The second is to drive the micro-actuators one at a time.

Sometimes, because of anisotropies in the behavior of the microplatform translation when both micro-actuators are functioning, see Ref. [21], for smooth and fine motion, the micro-actuators have to function one at a time. To produce such a motion, the operator of the master device translates the end-effector in the positive or negative direction in the X axis indicating the rotation velocity and direction of the micro-actuators and at the same time rotates the end-effector about the Y axis to indicate which micro-actuator should function.

Table 1 illustrates the presented input modes above. The "+"/"−" symbols denote a positive/negative rotational micro-actuator speed, the "↑" symbol denotes a micro-actuator speed increase, while "0" denotes that the corresponding micro-actuator is not influenced. During the MiIM phase, "1" denotes that the corresponding micro-actuator is functioning and "0" denotes that the micro-actuator is not functioning.

4.2 Second Communication Channel. In order to realize the second communication channel from the microrobot to the haptic mechanism, we define the following control phases. (a) The macroscopic control phase (MaCP), during which the haptic mechanism operator drives the microplatform toward the microtarget, in a coarse motion, and (b) the microscopic control phase (MiCP), in which the micromanipulation of the microtarget occurs in fine motion. Next, both phases are presented in detail. Again, the control phases can be selected from the software.

4.2.1 The Macroscopic Control Phase. During this control phase, no micromanipulation forces exist, and therefore, normally the haptic device would not apply forces to the operator. However, as discussed earlier, above a critical micro-actuator speed, the microrobot vibrates vertically and may even tip over. To indicate the limits of the permissible actuation speed, a spring force proportional to the haptic end-effector translation (and micro-actuator speed) is applied to the operator, see Fig. 4. This force is given by

$$f_{sp} = k(p - 5) \quad (2)$$

where p is the haptic device end-effector translation, see Fig. 3, and k is a variable spring constant. By experimentation, it was found that tipping occurs at about 85% of the maximum micro-actuator speed, depending on the ground type or platform mass. To signal this limit, a spring constant three times harder than before is employed above 85% of the maximum speed. To achieve a smooth transition, the spring constant changes according to an exponential function. The maximum force applied to the operator is set to be 5 N. This value is slightly under 15% of 35.5 N, which is the average maximum controllable force a female can produce with her wrist according to Tan et al. [22]. Measurements in Ref. [23] showed that humans exert forces of up to 15% of their maximum ability, without fatigue for a long period of time. Consequently, the chosen spring constant, k, is defined as follows:

$$k = \begin{cases} 0.33, & |p-5| \le 4.25 \\ e^{0.68(|p-5|-4.25)} - 0.66, & 5.0 \ge |p-5| > 4.25 \\ 1, & |p-5| > 5.0 \end{cases} \quad (3)$$

4.2.2 The Microscopic Control Phase. During this control phase, forces resulting from the micromanipulation are applied to the operator by the haptic device. As seen in Fig. 5, the microplatform following the operator commands comes into contact with the environment, e.g., pushes a micro-object. The developed force is measured, filtered, and fed by the haptic device, according to a suitable scaling function, to the operator's hand. The scaling factor depends (a) on the maximum force applied by the microrobot, (b) on the maximum force that the haptic mechanism can apply, and (c) on the maximum force that the operator can exert without fatigue for a long period of time (5 N). Although the haptic mechanism can apply larger forces, it is designed for applications that need a maximum force of this magnitude, see Ref. [19]. Furthermore, experiments in Ref. [24] showed that the maximum force that the microrobot exerts is not greater than 0.05 N, thus

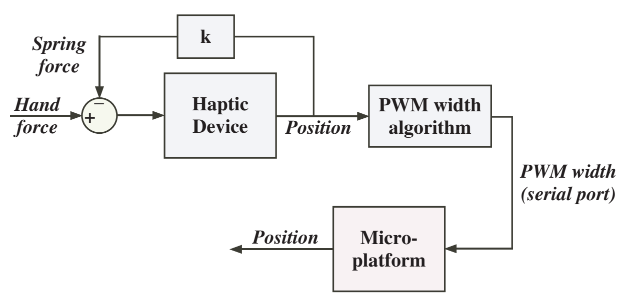

Fig. 4 The macroscopic control phase force loop

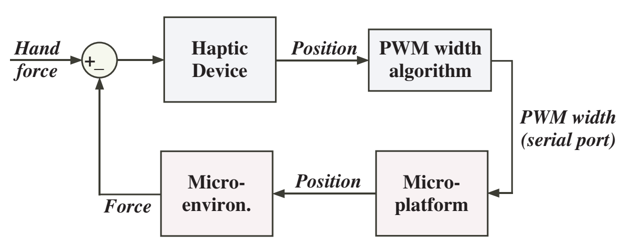

Fig. 5 The microscopic control phase force loop

Table 2 Function of the haptic telemanipulation environment modes and phases regarding the type of motion

	Coarse motion	Fine motion
1st communication channel	MaIM, MRIM	MiIM
2nd communication channel	MaCP	MiCP

Table 3 Definition of the symbols in Fig. 6 and Eq. (3)

Symbol	Definition
F	Operator's hand force
m_h	Operator's hand mass
b_h	Operator's hand damping
x_h	Operator's hand position
k_h	Operator's hand stiffness
m_m	Haptic mechanism mass
b_m	Haptic mechanism damping
x_m	Haptic mechanism position
k	Virtual spring constant

the selected scaling factor is 100. Oversampling at 1 kHz and the average calculation of successive samples before scaling was the filtering method employed.

In general, interaction forces are smooth. However, depending on the microrobot-environment springiness and damping, the generated forces can be in the form of impacts, [21]. In this case, a simple force magnification does not provide useful haptic information, while it may be potentially dangerous for both the operator and the haptic device. To overcome this situation, the impact forces are filtered and the resulting smooth signal is magnified and applied to the operator. As mentioned earlier, oversampling at 1 kHz and average calculation of successive samples were used. Although the magnitude of the impact forces can reach 0.3 N, the average value is about 20 times smaller, see Ref. [24] and the experimental results in Sec. 6.2.4. Hence, the same scale factor (100) was used.

Table 2 illustrates the function of the above modes and phases of the two communication channels regarding the type of motion (coarse or fine).

5 Haptic Telemanipulation Environment Simulation

Next, a 1-dof model system in macroscopic mode, with no interaction with the microenvironment, is defined. It consists of (a) the operator's hand, (b) the haptic mechanism, and (c) the microrobotic system, see Fig. 6(*a*). The operator's hand is modeled as a mass-spring-damper system, attached to the haptic mechanism, which is modeled as a mass-damper system, see Fig. 6(*b*). We do not present the model of the microplatform used here, since it is described in detail in Ref. [21]. Note that during the macroscopic control phase, the haptic device is connected with a virtual spring defined by Eq. (2), with spring constant k.

The transfer function of the "Hand+Haptic Device" system in Fig. 6 is described by Eq. (4), and the related symbols are defined in Table 3.

$$\frac{X_m(s)}{F(s)} = \frac{k_h}{m_h m_m s^4 + (m_h b_m + b_h m_m)s^3 + (m_h(k+k_h) + b_h b_m + k_h m_m)s^2 + (b_h(k+k_h) + k_h b_m)s + k_h k} \tag{4}$$

During the simulation the operator's hand mass m_h is 1.46 kg, the hand damping b_h is 3.6 N s/m, and the hand stiffness k_h is 200 N/m. These represent average values taken from the relevant literature [25,26]. The haptic mechanism apparent mass m_m in the X axis is about 0.27 kg and the mechanism damping b_m is about 5 N s/m. These values are found through experimentation with the haptic mechanism, see Ref. [19]. The input to the system is a step of about 0.18 N of the operator's hand force F. The virtual spring value k is 4 N/m. The simulated period is 20 s.

Figure 7 shows the result of the simulated try in MiIM under (MaCP). The operator's hand step force results in the translation of the haptic mechanism end-effector of about 0.045 m and the duty cycle command shown in Fig. 7 (first schema), as explained in Sec. 4.1.1. Consequently, when friction and inertia forces are

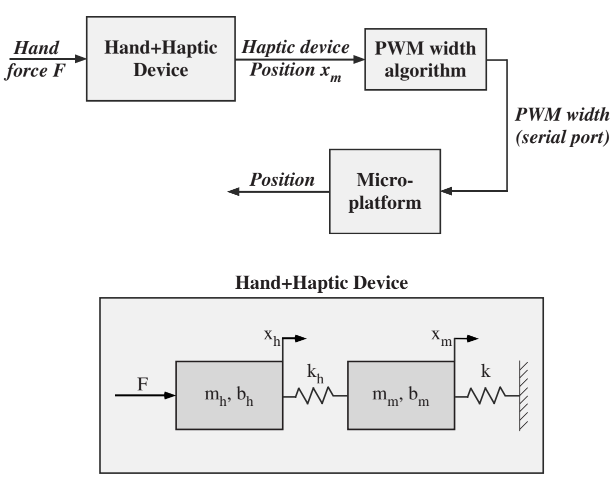

Fig. 6 The model of the haptic telemanipulation system including the user hand during the MaCP force loop (no interaction with the microenvironment)

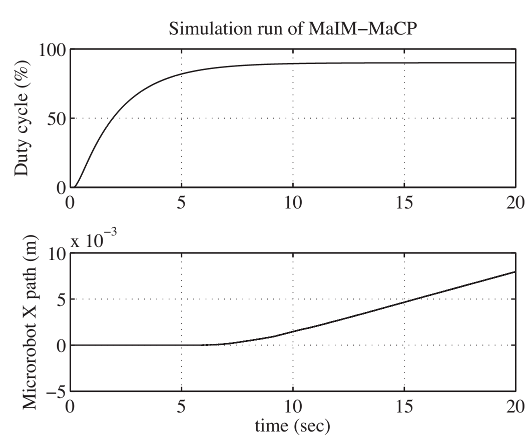

Fig. 7 The simulation result

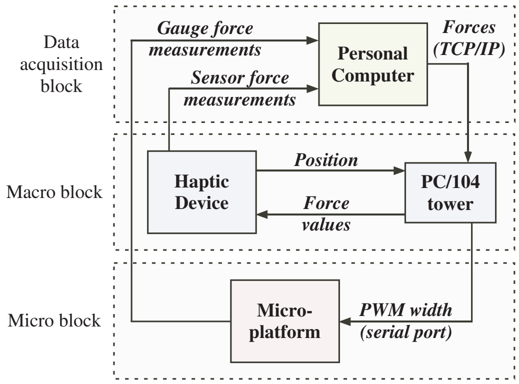

Fig. 8 The experimental setup

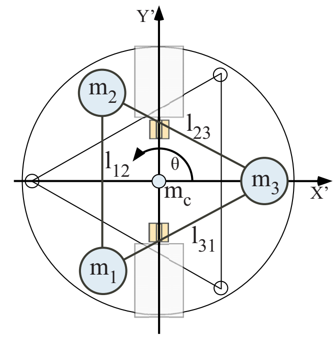

Fig. 9 Schematic view of the microrobot top with the white marks

exceeded (sixth second in Fig. 7), the microrobot starts to move, see the second schema in Fig. 7. Note here that after friction and inertia forces are exceeded, the microrobot can be driven with less speed.

6 Haptic Telemanipulation Environment Experiments

6.1 Experimental Setup. The experimental setup consists of three blocks, see Fig. 8. The first is the *Macroblock*, where the operator moves the haptic device end-effector along the X axis and rotates it about the Y axis. The end-effector position and the angle are captured by encoders attached on the haptic device actuators (Maxon dc motors), and transmitted to a PC/104 tower. This tower is the control unit, that runs the algorithm that translates the operator input into the microrobot input according to Eq. (1).

The *Microblock* consists of the microplatform, a 1 DOF strain gauge force sensor attached to it, and the PWM circuits. The input to the PWMs is transmitted from the PC/104 tower through a serial port. When the microrobot is about to perform a micromanipulation (e.g., the microrobot's end-effector is under a microscope's field of view) the operator changes the software operation to MiCP. In this case if the microrobot manipulates a micro-object, the strain gauge captures the produced microforces and transmits them to a PC in the *data acquisition block*. From there, these forces are passed to the PC/104 tower, and after suitable scaling and smoothing, the necessary commands are sent to the haptic device actuators by the PC/104 I/O card. The applied forces to the operator are measured by an ATI nano17 6DOF force sensor attached to the haptic device end-effector. These measurements are also passed to the data acquisition block.

In order to record the obtained microplatform trajectory during the experiments, we recorded a video the microplatform motion. To improve the results, white round marks were placed on the top surface of the microrobot. Figure 9 shows a schematic view of the microrobot top with the white marks, m_1, m_2, and m_3, and the platform center m_c.

The obtained video file is processed using Matlab's *image processing toolbox* routines to yield the coordinate trajectories of the white marks. Assuming these are placed on the three vertices of an isosceles triangle, we can calculate the angle θ according to

$$q = \left(\arcsin \frac{m_{1,y} - m_{3,y}}{\sqrt{(m_{1,x} - m_{3,x})^2 + (m_{1,y} - m_{3,y})^2}} \right) - 30 \text{ deg} \qquad (5)$$

and the coordinates of the microrobot center, $m_{c,x}$, $m_{c,y}$, according to

$$m_{c,x} = m_{1,x} + l_{m1c} \cos(30 \text{ deg} + q)$$

$$m_{c,y} = m_{1,y} - l_{m1c} \sin(30 \text{ deg} + q) \qquad (6)$$

where $m_{i,x}$ and $m_{i,y}$ are the coordinates of mark m_i $(1=1,2,3)$ and l_{m1c} is the distance between mark m_1 and the center m_c, according to

$$l_{m1c} = \frac{\sqrt{(m_{1,x} - m_{2,x})^2 + (m_{1,y} - m_{2,y})^2}}{2 \cos(30 \text{ deg})} \qquad (7)$$

The output of the processing is the trajectory of the microrobotic platform frame by frame. With a frame rate of 60 fps, a resolution of 1.7 pixels is achieved. In this case, where a 115.2 $\times 92.16$ mm^2 surface is covered by a frame of 720×576 pixels, the resolution is 0.3 mm, which is acceptable for the macroscopic mode. Note here that only two points (m_1 and m_3) are used in Eq. (5). Nevertheless, the third one is necessary in case of a rotation greater than 180 deg.

6.2 Experimental Results. We have executed five different experiments. The first four aimed at studying the behavior of the haptic telemanipulation environment during the three different input modes. The last one studies the forces applied to the operator by the haptic device during the contact between the microrobot and a rigid obstacle.

6.2.1 MaIM Experiment. Two experiments are executed in the MaIM input mode. In the first one, the master haptic device operator drives the microplatform in a straight line. The result is shown in Fig. 10. The left plot shows the output of the image processing algorithm. The right plots display the x, y, and θ coordinates of the microplatform's geometric center. We can see from the third plot at the right side of Fig. 10 that the operator has to make several correctional moves by rotating the microrobot. This is expected since the same command to the micro-actuators results in different rotational velocities due to several platform anisotropies, see Ref. [21]. The haptic command was between 65% and 75% of the maximum speed. In order to correct the translation, a $\pm 20\%$ difference between the two micro-actuator speeds was initiated.

In the second experiment, the master haptic device operator drives the microrobot along a curved path, see Fig. 11. This is achieved by rotating the haptic device end-effector by 25 deg about the Y axis, hence setting a 25% difference between the two micro-actuator speeds.

6.2.2 MRIM Experiment. In the MRIM experiment, equal but opposite micro-actuator speeds were set. The plus and minus arrows in Fig. 12 show the direction change, which is also visible on the plot of the angle θ of the microrobot at the right side. Observing the third plot on the right in Fig. 12, we observe that the microrobot rotates as commanded. The small translation that occurs is due to small differences between micro-actuator rotational speeds.

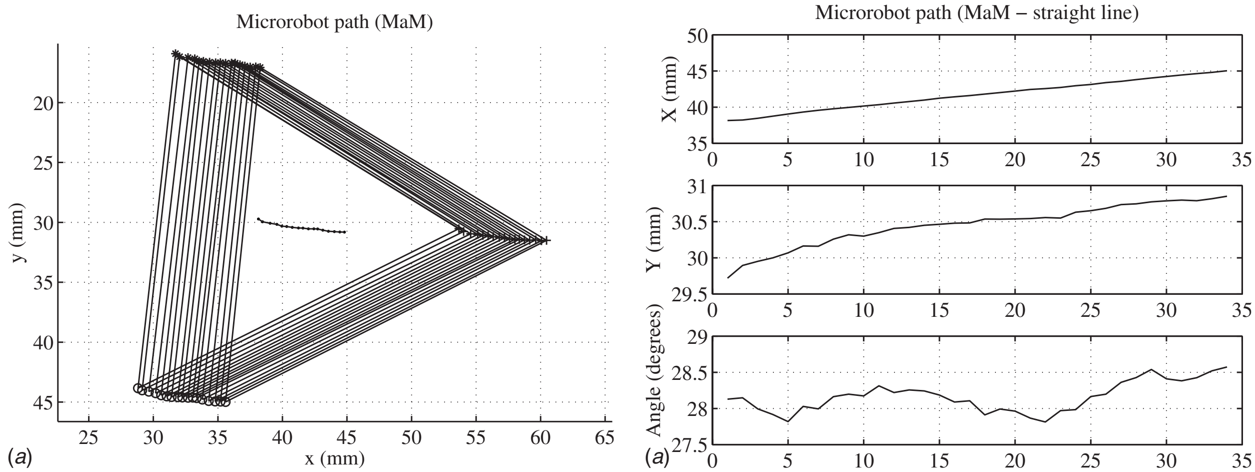

Fig. 10 The microrobot path during a MaIM experiment in a straight line

6.2.3 MiIM Experiment. The next two experiments study the microrobot motion in the MiIM mode. During the first try, the microplatform is driven at a low velocity and commanded by the master haptic device to move across the microscope's field of view. In Fig. 13 we see the tip of a needle attached on the microrobot. During this experiment, the command to both micro-actuators was about 55% of the maximum velocity.

During the second try, the micro-actuators are driven one at a time. Note here that in order to start the motion, the command to the micro-actuators should exceed 70–75% for a very short period because of frictional forces. This is addressed by a software routine, which when it is called, initiates such a command for a very

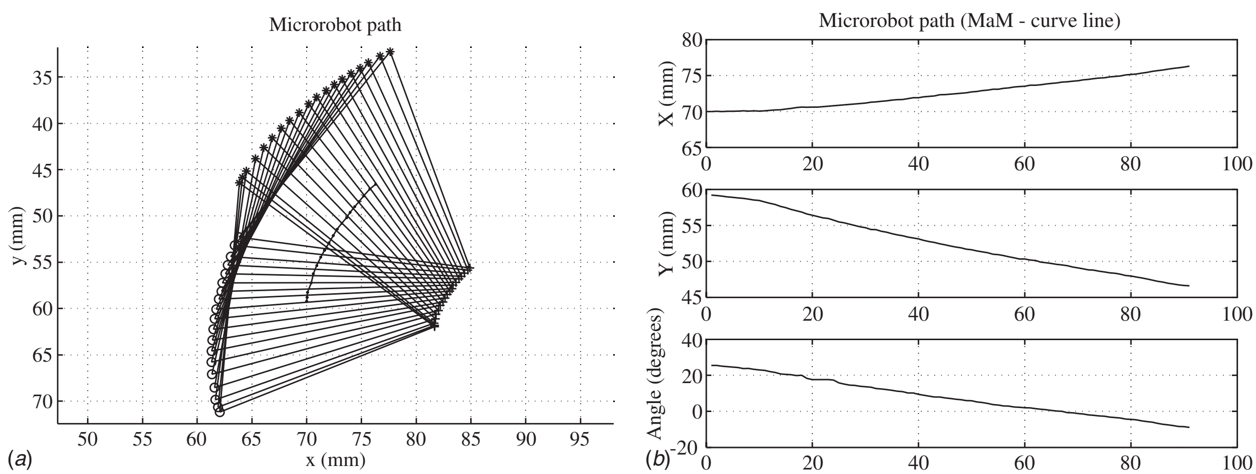

Fig. 11 The microrobot path during a MaIM experiment in a curved line

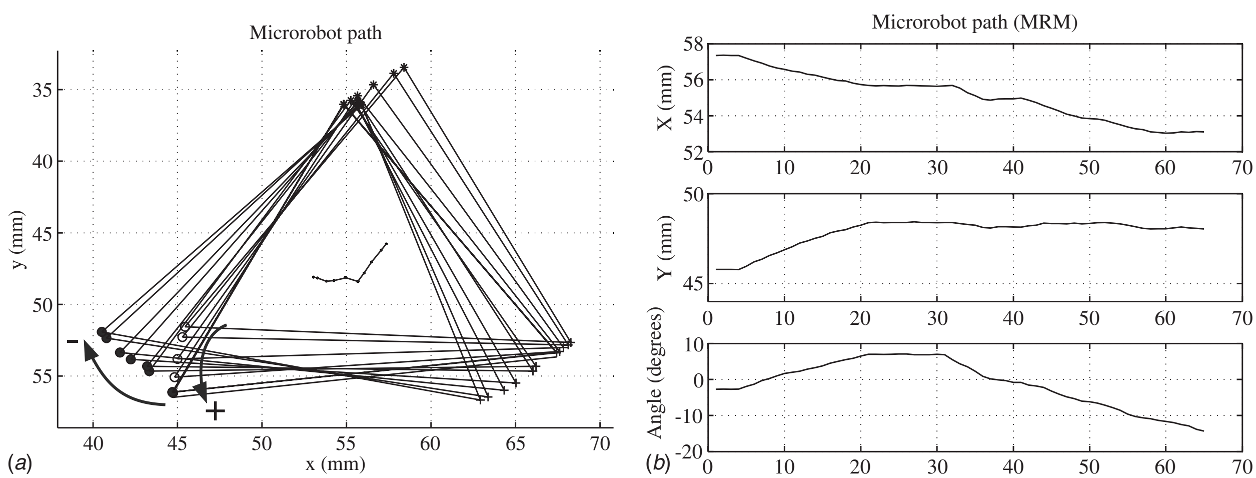

Fig. 12 The microrobot path during a MRIM experiment

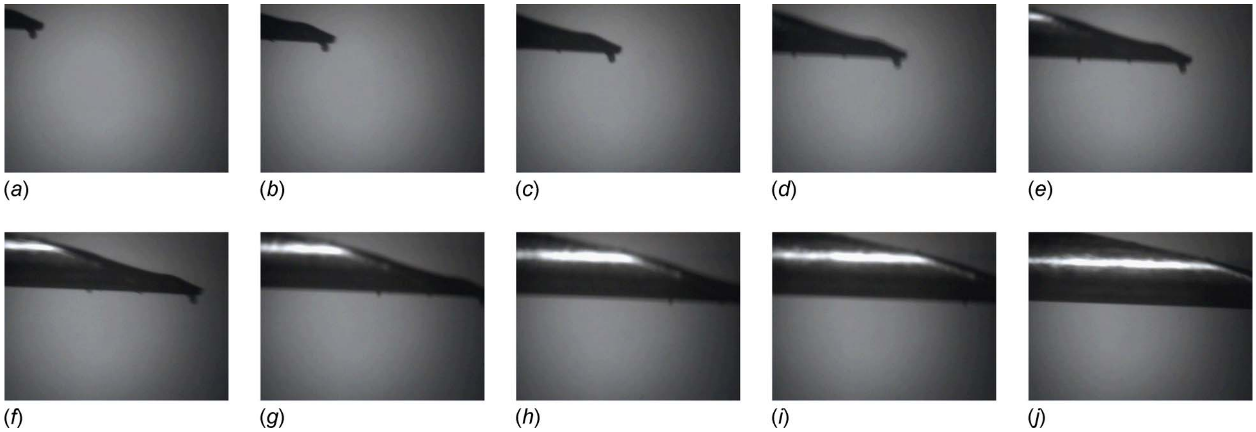

Fig. 13 Microrobot motion across the microscope field of view during a MiIM experiment (both actuators at a low speed)

short period and then returns to 50% of the maximum velocity. The result is shown in Fig. 14, where we can see the "slalom" motion of the platform. Both ways result in good behavior. However, the second one shows a smoother and finer motion.

The experiments showed that the operator should not decrease the command below 45% of the maximum speed because the micro-actuators stop due to friction. As before, to avoid platform tipping, the command should not exceed the 85–90%. The ideal operation space is between 55% and 85% depending on the input mode. These values depend on many environmental parameters, such as the type and the situation of the ground or the mass of the platform. However, these can be determined easily.

6.2.4 Force Experiments. The experiments described here study the forces applied to the operator by the haptic device during contact between the microrobot and a rigid obstacle. In the first experiment, the microrobot was always in contact and no impacts occur. The experiment was conducted with 70% and 80% of the maximum micro-actuator speeds and cover smooth and impact forces. Figure 15(*a*) shows the forces measured by a force sensor during micromanipulation before and after filtering and scaling.

In the second experiment because of the high stiffness of the obstacle, the measured forces are in the form of impacts, see Fig. 15(*b*). The top right plot shows in detail the impacts. By smoothing the signal and using the scaling factor defined in Sec. 3, the forces illustrated in Fig. 15(*b*) are obtained. Despite the impacts, the forces applied to the operator are smooth and meaningful, facilitating the force application to the obstacle.

Note that, in general, the stability of the system is an important issue, especially for the master haptic device. However in our case, the interaction forces are in general low and smooth as they correspond to a soft environment, due to the microrobot-environment springiness and damping [24]. Even in the case of mild impact forces, these are filtered and the resulting smooth signal is magnified and applied to the operator. The filtering itself does not introduce a significant delay and therefore it does not destabilize the system, see Fig. 15.

7 Conclusions

The analysis and several experimental results of a new haptic telemanipulation environment are presented in this paper. The proposed environment combines and controls a 5DOF force feedback mechanism, acting as the master, and a 2DOF microrobot, acting as the slave. Regardless of the disparity between the master and slave and the fact that the slave microrobot is driven by two centripetal force vibration micromotors, the environment gives to the operator the ability to drive and control the microplatform in a functional and simple manner.

The proposed environment manages to solve with success problems that arise during the haptic micromanipulation of the specific device, such as the fact that the slave microplatform and the master haptic device are kinematically dissimilar, that the vibration actuators must operate within a specific speed range (rpm) and at the same time achieve a high speed in macroscopic motion and

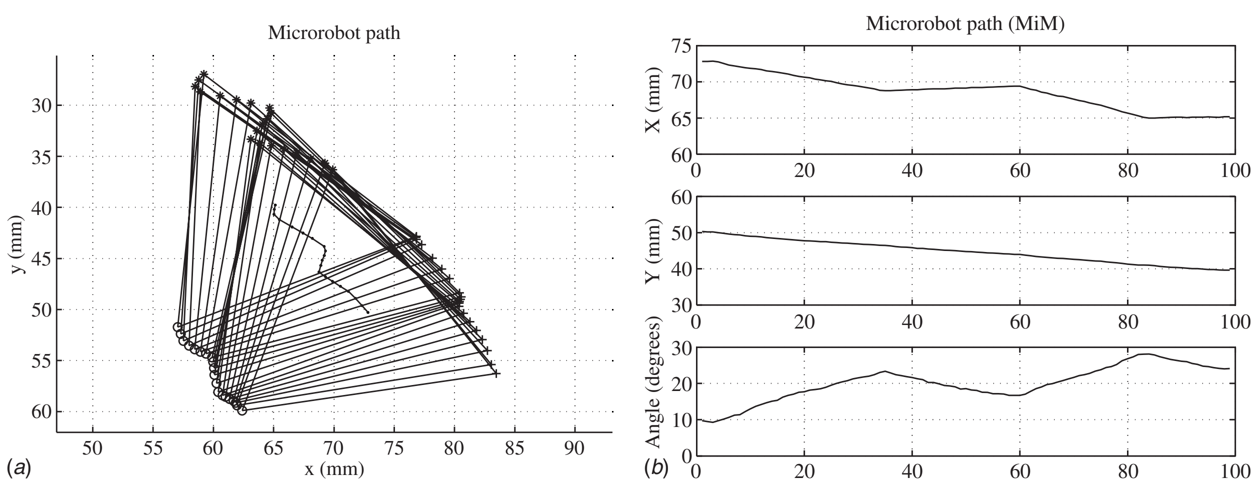

Fig. 14 The microrobot path during a MiIM experiment (actuators one at a time)

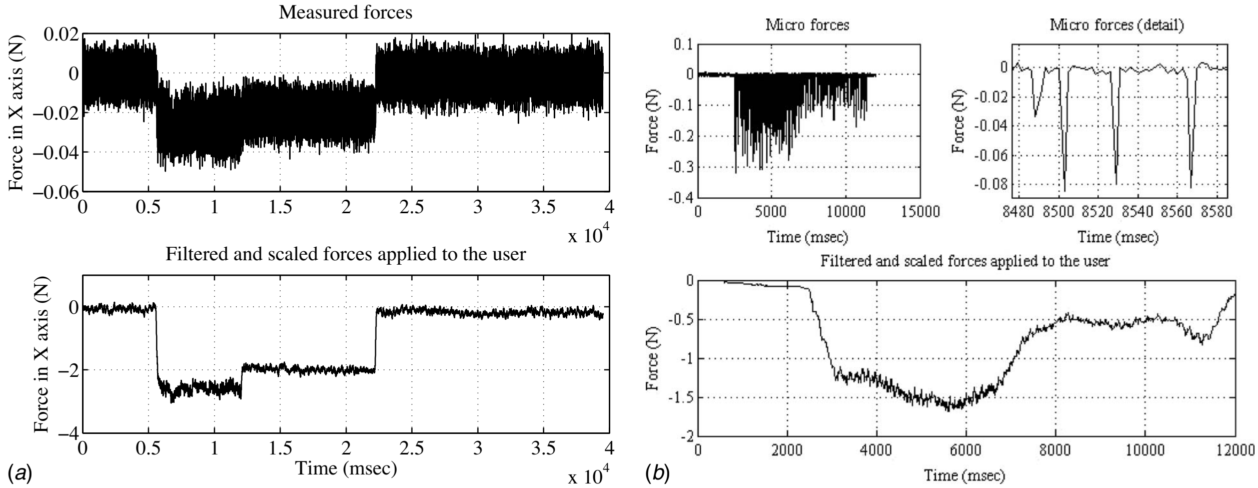

Fig. 15 The smooth (*a*) and impact (*b*) forces applied to the operator with and without filtering and scaling

submicrometer positioning accuracy in microscopic motion. In addition, even though the microforces measured by the microrobot can be in the form of impacts, the forces applied to the operator are smooth and meaningful, facilitating the force application to the obstacle.

Acknowledgment

The authors would like to thank Dr. P. Vartholomeos for his assistance in setting up the microrobotic environment.

References

[1] Salcudean, S. E., Ku, S., and Bell, G., 1997, "Performance Measurement in Scaled Teleoperation for Microsurgery," *Proceedings of the First Joint Conference in Computer Vision, Virtual Reality and Robotics in Medicine and Medial Robotics and Computer-Assisted Surgery (CVRMed-MRCA '97)*, Grenoble, France, pp. 789–798.

[2] Salcudean, S. E., and Yan, J., 1994, "Towards a Force-Reflecting Motion-Scaling System for Microsurgery," Proceedings of the IEEE Int. Conf. on Robotics and Automation (ICRA'94), San Diego, CA, pp. 2296–2301.

[3] Salcudean, S. E., Wong, N. M., and Hollis, R. L., 1995, "Design and Control of a Force-Reflecting Teleoperation System With Magnetically Levitated Master and Wrist," IEEE Trans. Rob. Autom., **11**(6), pp. 844–858.

[4] Sitti, M., and Hashimoto, H., 1998, "Tele-Nanorobotics Using Atomic Force Microscope," *Proceedings of the IEEE/RSJ International Conference on Intelligent Robots and Systems*, Victoria, BC, Canada, pp. 1739–1746.

[5] Kwon, D. S., Woo, K. Y., and Cho, H. S., 1999, "Haptic Control of the Master Hand Controller for a Microsurgical Telerobot System," *Proceedings of the IEEE International Conference on Robotics and Automation (ICRA '99)*, Detroit, MI, pp. 1722–1727.

[6] Ando, N., Ohta, M., and Hashimoto, H., 2000, "Micro Teleoperation With Haptic Interface," *Proceedings of 2000 IEEE International Conference on Industrial Electronics, Control and Instrumentation (IECON2000)*, Nagoya, Japan, pp. 13–18.

[7] Massie, T., and Salisbury, J. K., 1994, "The Phantom Haptic Interface: A Device for Probing Virtual Objects," *Proceedings of the ASME Winter Annual Meeting, Symposium on Haptic Interfaces for Virtual Environment and Teleoperator Systems*, Chicago, IL, pp. 295–301.

[8] Menciassi, A., Eisinberg, A., Carrozza, M. C., and Dario, P., 2003, "Force Sensing Microinstrument for Measuring Tissue Properties and Pulse in Microsurgery," IEEE/ASME Trans. Mechatron., **8**(1), pp. 10–17.

[9] Sitti, M., Aruk, B., Shintani, H., and Hashimoto, H., 2003, "Scaled Teleoperation System for Nano-Scale Interaction and Manipulation," Adv. Rob., **17**(3), pp. 275–291.

[10] Ammi, M., and Ferreira, A., 2005, "Realistic Visual and Haptic Rendering for Biological-Cell Injection," *Proceedings of the IEEE International Conference on Robotics and Automation (ICRA '05)*, Barcelona, Spain, pp. 930–935.

[11] Mattos, L., Grant, E., and Thresher, R., 2006, "Semi-Automated Blastocyst Microinjection," *Proceedings of the IEEE International Conference on Robotics and Automation (ICRA '06)*, Orlando, FL pp. 1780–1785.

[12] Kortschack, A., Shirinov, A., Trueper, T., and Fatikow, S., 2005, "Development of Mobile Versatile Nanohandling Micro-Robots: Design, Driving Principles, Haptic Control," Robotica, **23**(4), pp. 419–434.

[13] Grange, S., Conti, F., Helmer, P., Rouiller, P., and Baur, C., 2001, "The Delta Haptic Device as a Nanomanipulator," Proc. SPIE, **4568**, pp. 100–111.

[14] Colgate, J. E., 1991, "Power and Impedance Scaling in Bilateral Manipulation," *Proceedings of the IEEE International Conference on Robotics and Automation (ICRA '91)*, Sacramento, CA, pp. 2292–2297.

[15] Goldfarb, M., 1998, "Dimensional Analysis and Selective Distortion in Scaled Bilateral Telemanipulation," *Proceedings of the IEEE International Conference on Robotics and Automation (ICRA '98)*, Leuven, Belgium, pp. 1609–1614.

[16] Lu, Z., Chen, P. C. Y., Ganapathy, A., Zhao, G., Nam, J., Yang, G., Burdet, E., Teo, C., Meng, Q., and Lin, W., 2006, "A Force-Feedback Control System for Micro-Assembly," J. Micromech. Microeng., **16**(9), pp. 1861–1868.

[17] Park, J., and Khatib, O., 2006, "A Haptic Teleoperation Approach Based on Contact Force Control," Int. J. Robot. Res., **25**(5–6), pp. 575–591.

[18] Faulring, L. E. et al., 2007, "Haptic Display of Constrained Dynamic Systems Via Admittance Displays," IEEE Trans. Rob. Autom., **23**(1), pp. 101–111.

[19] Vlachos, K., Papadopoulos, E., and Mitropoulos, D., 2003, "Design and Implementation of a Haptic Device for Urological Operations," IEEE Trans. Rob. Autom., **19**(5), pp. 801–809.

[20] Vlachos, K., and Papadopoulos, E., 2006, "Transparency Maximization Methodology for Haptic Devices," IEEE/ASME Trans. Mechatron., **11**(3), pp. 249–255.

[21] Vartholomeos, P., and Papadopoulos, E., 2006, "Analysis, Design and Control of a Planar Micro-Robot Driven by Two Centripetal-Force Actuators," *Proceedings of the IEEE International Conference on Robotics and Automation (ICRA '06)*, Orlando, FL, pp. 649–654.

[22] Tan, H. Z., Srinivasan, M. A., Ederman, B., and Cheng, B., 1994, "Human Factors for the Design of Force-Reflecting Haptic Interfaces," ASME Dyn. Syst. Control Div., **55**(1), pp. 353–359.

[23] Wiker, S. F., Hershkowitz, E., and Zilk, J., 1989 "Teleoperator Comfort and Psychometric Stability: Criteria for Limiting Master-Controller Forces of Operation and Feedback During Telemanipulation," Vol. I, *Proceedings of the NASA Conference on Space Telerobotics*, Pasadena, CA, pp. 99–107.

[24] Vartholomeos, P., Vlachos, K., and Papadopoulos, E., 2007, "On the Force Capabilities of Centripetal Force-Actuated Microrobotic Platforms," *Proceedings of the IEEE International Conference on Robotics and Automation (ICRA '07)*, Roma, Italy, pp. 1116–1121.

[25] Gil, J. J., Avello, A., Rubio, A., and Florez, J., 2004, "Stability Analysis of a 1 DOF Haptic Interface Using the Routh–Hurwitz Criterion," IEEE Trans. Control Syst. Technol., **12**(4), pp. 583–588.

[26] Salcudean, S. E., Zhu, M., Zhu, W.-H., Hashtrudi-Zaad, K., 2000, "Transparent Bilateral Teleoperation Under Position and Rate Control," Int. J. Robot. Res., **19**(12), pp. 1185–1202.

AUTHOR QUERIES — 008804CIS

#1 Au: Please check our change from ″able″ to ″enabled.″

#2 Au: Please check our change from ″have″ to ″be in.″

#3 Au: Please define ″PWM″ if possible.

#4 Au: Please check our change from ″have″ to ″be in″.

#5 Au: Please check our change from ″in″ to ″to.″

#6 Au: Please check our change from ″video record″ to ″recorded a video″.

#7 Au: Please check our change from ″have″ to ″are in″.

#8 Au: Please check our change from ″have″ to be in.″

#9 Au: Please supply full list of authors for the journal in Ref. 18.